APPLICATION OF TRACE-BASED SPECTRAL PRINCIPAL COMPONENT ANALYSIS METHOD FOR SEISMIC THIN-LAYER THICKNESS DELINEATION

JIAN ZHOU [1,2,3], JING BA[1]*, JOHN P. CASTAGNA [2] and JOSÉ M. CARCIONE [1,4]

[1] *Hohai University, Nanjing 211100, P.R. China. * jba@hhu.edu.cn; jingba@188.com*
[2] *University of Houston, Houston, Texas 77204, U.S.A.*
[3] *Nanjing Foreign Language School Fangshan Campus, Nanjing, 211199 China.*
[4] *Istituto Nazionale di Oceanografia e di Geofisica Sperimentale, Borgo Grotta Gigante 42c, 34010 Sgonico, Trieste, Italy.*

ABSTRACT

Zhou, J., Ba, J., Castagna, J.P. and Carcione, J.M., 2019. Application of trace-based spectral principal component analysis method for seismic thin-layer thickness delineation. *Journal of Seismic Exploration*, 28: 551-576.

Spectral decomposition of a 3-dimensional reflection seismic volume generates large volumes of spectral data in the form of time-frequency analysis at every seismic signal location. Conventional spectral principal component analysis (PCA) compresses the multi-dimensional spectral data exclusively on amplitude maps at interpreted seismic horizon. This overlooks the time-variant nature of spectral amplitudes. Hence, it is difficult to estimate thin-layer thickness variations directly from the conventional horizon-based spectral PCA (HSPCA) results. A trace-based spectral principal component analysis (TSPCA) method is proposed for seismic thin-layer thickness delineation. Compared to HSPCA, TSPCA calculates spectral principal components (PCs) within a time window over the targeted seismic event on a trace-by-trace basis. Trace-based spectral PCs are assumed independent, i.e., as amplitude responses from reflection events with different frequency characteristics. A rotation of PC coefficients following the Varimax criterion is proposed to automatically interpret the three most significant spectral PCs as related to (1) reflection amplitude determined by rock impedances, (2) tuning of a pure even-reflection pair, or (3) tuning from a pure odd-reflection pair. The latter two types of tuning-related amplitude are both governed by thin-layer thickness and have different frequency responses. Results on synthetic wedge models of pure odd- and even-reflection pair thin layers show that the trace-based spectral PCs show a distinct relationship to thin-layer thickness. Comparing spectral PC images calculated on a geologically complex 3D model after HSPCA and TSPCA methods, we conclude that TSPCA has superior capability for precise thickness delineation, especially for subtle thickness variations in the model.

KEY WORDS: spectral decomposition, HSPCA, TSPCA.

INTRODUCTION

Due to the complex propagation behavior of seismic waves in anelastic Earth media, seismic reflection signal has limited time- and frequency-resolutions. As targets become increasingly thinner, seismic signal processing methods need to overcome the problem of inadequate resolution before a robust thin-layer thickness estimation can be made.

Spectral decomposition is a popular seismic signal processing and interpretation technique that can potentially improve seismic resolution (Cohen, 1989; Gao et al., 1999; Gholami, 2013). It has been widely applied to interpret frequency-dependent seismic responses, e.g. fluid-induced reflectivity variation and lithology changes (Castagna et al., 2003; Korneev et al., 2004; Sinha et al., 2005; Chen et al., 2008; Williams and Chadwick, 2012; Carcione et al., 2018). More commonly, based on the understanding that narrow-band seismic data better delineate the seismic "tuning" pattern at individual frequencies, features of specific thickness that correspond to the tuning frequency is highlighted in the iso-frequency images (Partyka et al., 1999). However, one of the problems after the spectral decomposition is that the volume of seismic data increases and interpreting the spectral volumes becomes time consuming. Moreover, the choice of the frequency that best represents the true geology can be arbitrary (Marfurt and Kirlin, 2001). Using specifically designed seismic attributes extracted from spectral data volumes, one can delineate some geologic features. For example, using peak-amplitude, peak-frequency and coherence attributes gives a better visualization of channel features (Marfurt and Kirlin, 2001; Liu and Marfurt, 2007), and amplitude ratios of frequency components are indicative of thickness variations (Khare and Martinez, 2008; Nowak et al., 2008). However, much of the information in the spectral volumes is not exploited by these spectral attribute methods.

Taking advantage of the clustering behavior in spectral data volumes can reduce data volumes without losing vital information (Wang, 2012). Principal component analysis (PCA) is an effective multi-variant statistical method that compresses high-dimension data while removing random noises (Jolliffe, 2002; Jolliffe and Cadima, 2016; Chen et al., 2017). It reduces data redundancy by projecting input data to directions in hyperspace where variations are most significant. Firstly, PCA of spectral data from time-frequency analysis preserves most variances in spectrally-decomposed 3D data volumes (Roden et al., 2015). On the other hand, spectral data projected, based on eigenvectors, are orthogonal-linear combinations of individual frequencies ranked by the variance of the data that they account for, suggesting that each PC is independent (Guo et al., 2009). Due to the superiority of orthogonal attributes, PCA could aid in multiple regression, and provides independent visualizations of the geology, with PC potentially highlighting different geological features (Honorio et al., 2014; Zhou et al., 2014). Conventional horizon-based spectral PCA takes spectral amplitude

from sample points exclusively along a seismically picked 2D horizon, and process all points altogether regardless of their spatial distribution. On one hand, this arrangement focuses on the overall amplitude-distribution trend along the picked seismic event, possibly representing the targeted thin layer. In this sense, spectral PCA essentially acts as a compressor and noise filter for high-dimensional spectral data. On the other hand, using only spectral amplitude at a 2D horizon limits the ability of PCA for extracting time-variant information embedded in the original spectral data (Guo et al., 2009), for example layer thickness (Partyka et al., 1999). Furthermore, relying heavily on amplitude at picked horizons requires the error in horizon picks to be relatively small, which is not very common in cases with complex geology, where the horizontal heterogeneity is strong.

In this work, a trace-based spectral PCA (TSPCA) algorithm is proposed for thin-layer thickness delineation. Compared to the conventional horizon-based spectral PCA (HSPCA), TSPCA takes advantage of the correlation relationships between spectral iso-frequency traces. The trace-based PCA of spectral amplitude is essential to decompose the original signal into independent responses of rock impedance contrasts and thin-layer tuning effects based on the characteristic frequencies for each trace. In addition, Varimax rotation of PC coefficients is explored as a tool for automated interpretation of spectral PCs. The Varimax criterion (Kaiser, 1958), when applied in seismic signal analysis, aids in improving data spikiness, zero-phase correlation, and image focusing (Wiggins, 1978; Levy and Oldenburg, 1987; Fomel et al., 2007). In this workflow, using Varimax-rotated PC coefficients as a function of frequency enables automated interpretation of spectral PCs and differentiation of amplitude responses with different frequency characteristics.

The paper is organized as follows. First, the TSPCA approach is compared against the conventional HSPCA for thin-layer thickness delineation. Then, the Varimax criterion is demonstrated as an aid in interpreting spectral PCs for individual traces, which is essential for automated PC image generation. Effectiveness of the TSPCA in thickness delineation is tested using two wedge models and a geologically complex 3D model consisting of an incised valley and turbidite channel to show its superior performance over conventional HSPCA.

THEORY AND METHODS

A. Principal Component Compression and Decomposition

PCA for data compression is often considered a low-rank approximation of the high-redundancy original dataset (Chen et al., 2017; Sun and Du, 2018). One of the common algorithms of PCA is the covariance method. In this algorithm, the key process is the eigendecomposition of the

covariance matrix of input dataset (**D**). Since the correlation matrix is equivalent to the covariance matrix normalized by the mean values of variables, it is used here for simplicity.

The correlation matrix (*r*) is always diagonalizable. Using eigendecomposition, the *r* matrix can be expressed as the sum of its eigenvalues (λ) multiplied by the corresponding eigenvectors (*V*) and the transpose of each eigenvector (V^T):

$$r = \sum_{i=1}^{m} \lambda_i V_i V_i^T \quad , \tag{1}$$

where *m* indicates the number of variables. Ranking eigenvalues from high to low indicate the largest and smallest amount of variance represented by each principal component (PC). Usually PCs associated with the largest few *p* eigenvalues ($p \ll m$) are large enough to be significant. The original *r* matrix can be approximated by $\hat{r}$ where non-significant terms are excluded without losing much variance:

$$\hat{r} = \sum_{i=1}^{p} \lambda_i V_i V_i^T \approx r \quad . \tag{2}$$

By incorporating the scalar λ into the two matrices *V* and V^T, (2) can be rewritten as:

$$\hat{r} = \hat{R}\hat{R}^T \approx r \tag{3}$$

where

$$\hat{R}_i = \sqrt{\lambda_i} V_i \tag{4}$$

and *i* ranges from 1 to *p*. The value of *p* depends on the degree of redundancy in the dataset, which will be discussed in a following section.

The second application of PCA is for decomposing the original dataset into a selected number of subsets based on the most significant directions in data hyperspace. Because PCs are geometrically orthogonal, they are considered independent of each other (Sun and Du, 2018). Individual PCs are calculated by projecting the standard-score form (*z*-score) of the original data using V^T as coefficients:

$$PC_i = V_i^T z \quad , \tag{5}$$

where *i* ranges from 1 to *p*. However, there is one apparent problem for the principal component decomposition. Directly associating PCs to data in real measurement space is often difficult (Guo et al., 2009). This problem will be addressed in sections below.

B: Horizon- and Trace- Based Spectral PCA

Conventional spectral PCA treats amplitudes from a pre-selected 2D seismic horizon at different frequencies as different input variables. By calculating the most significant spectral PCs, variations in the spectral amplitudes are extracted while random noises are removed. Fig. 1 illustrates the workflow of the conventional horizon-based spectral PC analysis (HSPCA). The general procedure can be summarized in the following steps:
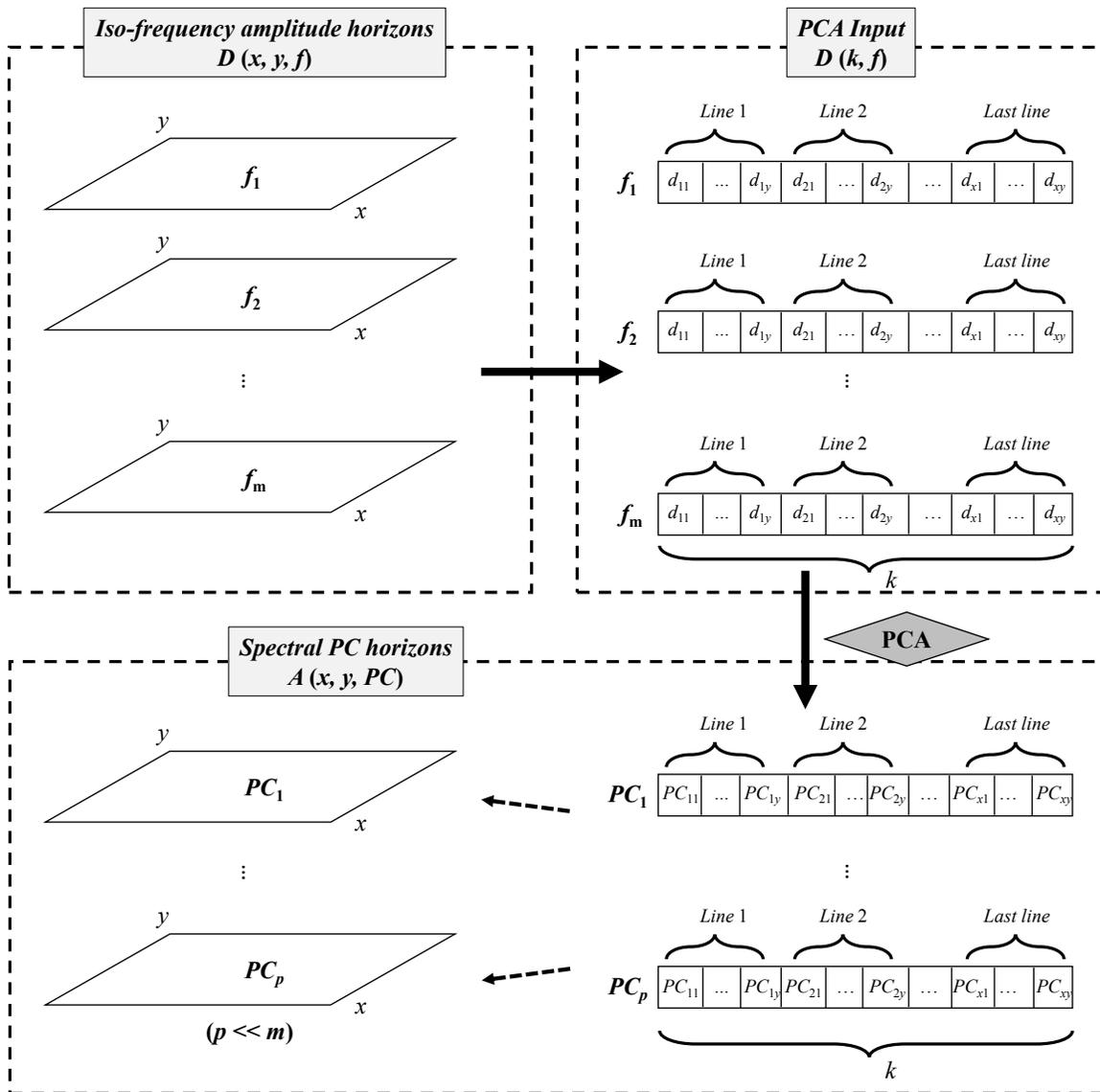
Fig. 1. Conventional HSPCA method.

(1) Define a seismic event where a thin layer is located;
(2) Extract iso-frequency amplitude horizons from *m* iso-frequency amplitude cubes generated by any spectral decomposition algorithm;

(3) Balance iso-frequency amplitudes from different frequencies to remove the wavelet shape influence on amplitude (Liu and Marfurt, 2007);

(4) Sort all points from each 2D iso-frequency horizon into 1D strings, then compile all iso-frequency amplitudes as matrix **D**;

(5) Perform PCA on matrix **D**, then reorganize outputted p spectral PCs back to p 2D PC horizons.

One advantage of this algorithm is that it only needs one PC analysis for each seismic horizon, hence the efficiency of calculation is relatively high. Statistically, it makes no difference how spectral amplitudes are inputted into matrix **D** before PCA. However, performing PCA to amplitudes from only one time-sample at a pre-selected seismic horizon ignores useful information hidden in spectral amplitude variation as a function of time, including layer thickness, which is an important reason for time-frequency analysis in the first place. To deal with with this issue, a trace-based spectral PCA (TSPCA) is proposed here to take advantage of both the time- and frequency- domain information carried in iso-frequency amplitude data generated by spectral decomposition.
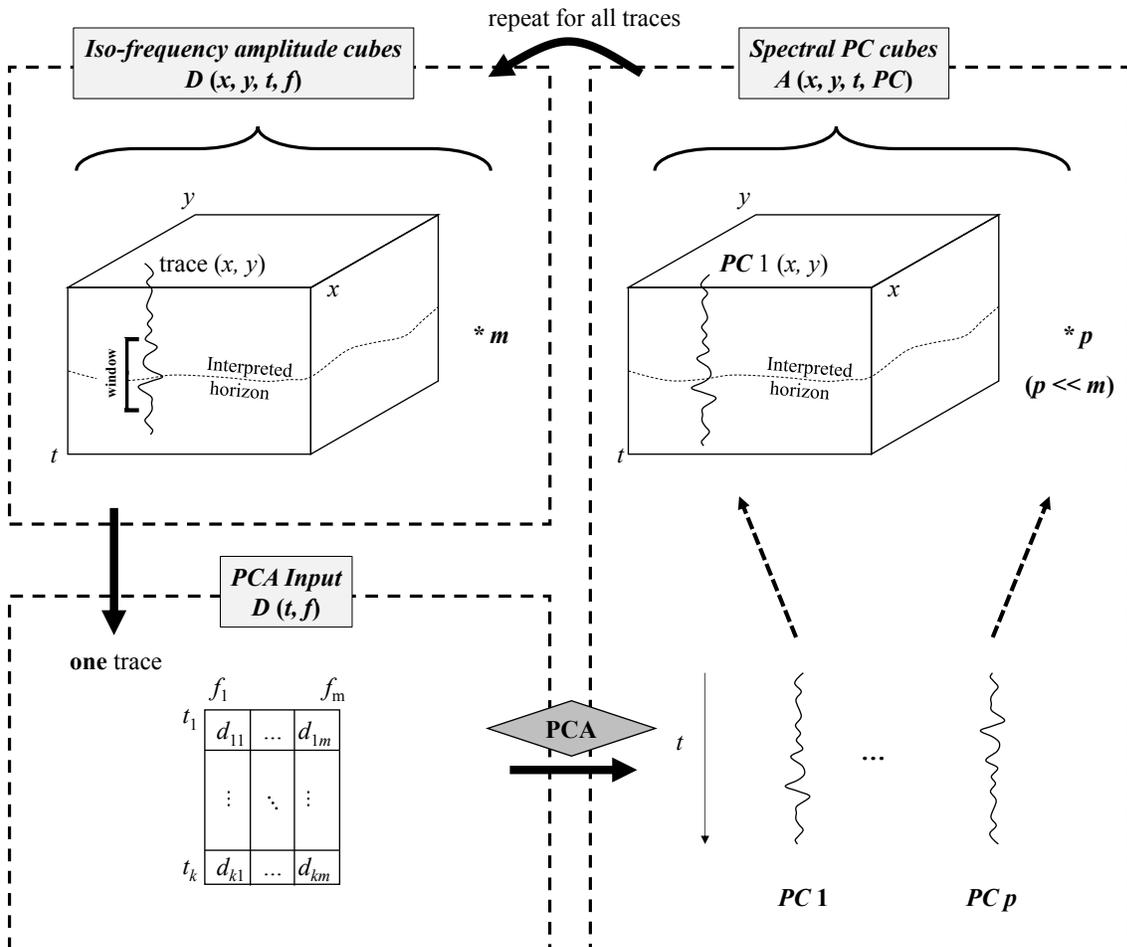

Fig. 2. TSPCA method.

Different from the conventional HSPCA, the TSPCA algorithm calculates the PC outputs on a trace-by-trace basis. Fig. 2 illustrates the workflow of the TSPCA. The general procedure can be summarized as:

(1) Define a time window whose center is located at the seismic interface of interest;
(2) Extract iso-frequency traces from m iso-frequency amplitude cubes outputted from any spectral decomposition algorithm;
(3) Balance spectral amplitudes at different frequencies to remove the wavelet shape influence (Liu and Marfurt, 2007);
(4) Compile balanced spectral traces into matrix $\boldsymbol{D}$;
(5) Perform PCA on matrix $\boldsymbol{D}$, then reorganize outputted p spectral PCs back to 1D PC traces. Record PC amplitudes at the center of the windowed trace to the corresponding points at "x" and "y" location of the p PC horizon images.
(6) Repeat steps (1) through (5) until all points on the horizon are processed.

C: Interpretability of TSPCs by Varimax Rotation

One of the reasons to perform spectral PCA on a trace-by-trace basis is that it enables interpretation of time-frequency data directly for individual traces. This is achievable via interpreting PC coefficients ($\boldsymbol{V}$) and individual corresponding outputted spectral PC amplitudes. Based on (3), $\hat{r}$ is equivalent to the $\hat{R}$ matrix multiplied with its transpose. However, this equation is not necessarily unique. There are an infinite number of orthogonal p-by-p matrices $\boldsymbol{X}$, where

$$XX^T = I \tag{6}$$

that satisfies:

$$\hat{r}_v = (\hat{R}X)(X^T \hat{R}^T) = \hat{r}_v. \tag{7}$$

Here X is effectively a rotation of the $\hat{R}$ matrix. Each X corresponds to a specific rotation to $\hat{R}$. The purpose of rotating matrix $\hat{R}$ is to make it easier for interpretation of each PC in (4).

The Varimax criterion is one of the most common methods for orthogonal matrix rotation. The aim is to rotate the matrix so that variation in all the columns is as large as possible. The Varimax criterion is selected because it preserves the orthogonality of the $\hat{R}$ matrix, hence it is reversible. A general expression of the Varimax criterion (Kaiser, 1958) is given as:

$$\hat{R}_v = \arg\max \left(\sum_{j=1}^{m} \sum_{i=1}^{p} \left(\Lambda\hat{R} \right)_{ij}^4 - \frac{1}{p} \sum_{j=1}^{m} \left(\sum_{i=1}^{p} \left(\Lambda\hat{R} \right)_{ij}^2 \right)^2 \right) , \qquad (8)$$

where Λ indicates variance. Generally, coefficients in $\hat{R}$ obtained from the covariance matrix needs to be scaled before rotation. However, since our $\hat{r}$ matrix is created by using correlation coefficients, which is a normalized covariance, the scaling is already done.

There are multiple methods capable of solving for $\hat{R}_v$. One of the conceptually simple algorithms is to iteratively perform bivariate rotations. Each iteration begins with selection of two columns in the m-by-p $\hat{R}$ matrix, $\hat{R}_i$ and $\hat{R}_j$, which defines a two-dimensional plane within the p-dimension hyperspace. Next, calculate the angle for rotation in the selected 2D plane using the following (Kaiser, 1958):

$$\phi = \frac{1}{4} \tan^{-1} \frac{2n \sum AB - 2 \sum A \sum B}{p \left[\sum \left(A^2 - B^2 \right) \right] - \left(\sum A^2 - \sum B^2 \right)} \qquad (9)$$

where

$$A = \hat{R}_i^2 - \hat{R}_j^2$$

and

$$B = 2\hat{R}_i \hat{R}_j \quad .$$

Then, rotating the selected two columns by multiplying $\hat{R}$ to rotation

matrix $\begin{pmatrix} \cos\phi & -\sin\phi \\ \sin\phi & \cos\phi \end{pmatrix}$. Afterwards data points in this 2D plane have the

highest variation along the new axes, i.e., are they are closest to the two axes.

The iteration ends when rotations are performed on all C_2^p pairs of columns,

since i ranges from 1 to p, and j ranges from $(i+1)$ to p. More iterations are performed until the Varimax criterion is met in all p dimensions (columns)

in $\hat{R}$, i.e. a small enough rotation angle is reached. Another algorithm that is

computationally more efficient is the singular value decomposition (SVD) of
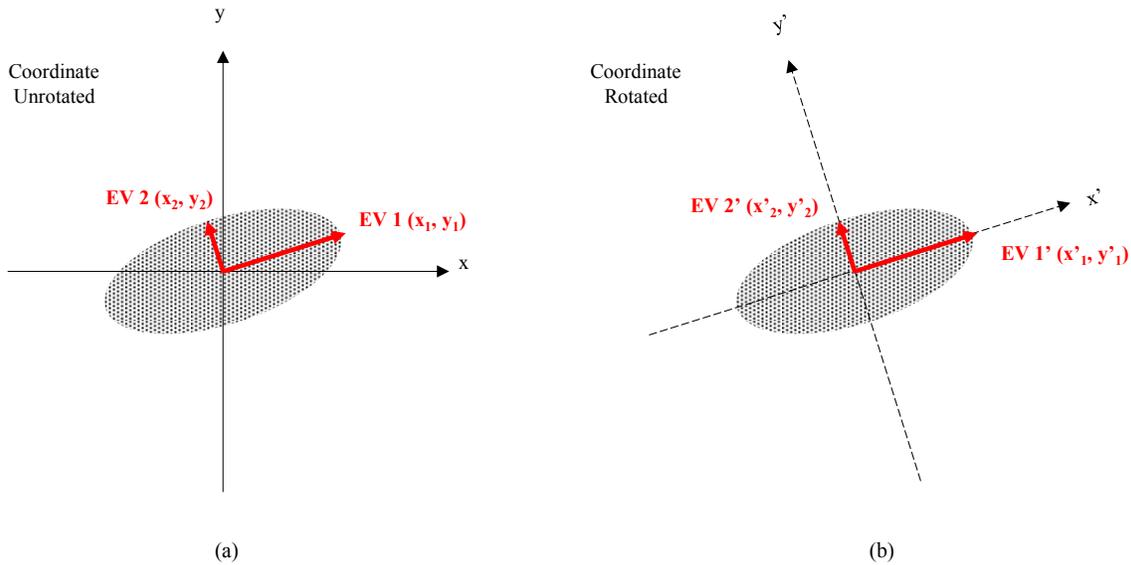
$\hat{R}$ (Lawley and Maxwell, 1971).

Fig. 3. (a) PCA of input data. (b) Varimax rotation of PC coordinates. EV indicates eigenvector, dotted area indicates input data points.

A schematic is shown in Fig. 3 to compare the procedure of (a) calculating the PC coefficients following (3) by eigendecomposition, and (b) rotating the selected p columns to obtain the maximum variation following (7). After the Varimax rotation, coefficients in $\hat{R}_v$ have maximum variations along the new axes. Conceptually this means that the coefficients at all m frequencies scatter close to the new axes in the p-dimension hyperspace ($\hat{R}_v$), suggesting a higher interpretability than the original coefficients in $\hat{R}$ [Fig. 3(b)]. Driving $\hat{R}$ values towards either zero or their maximum possible absolute value (scaled to unity) helps to differentiate, in rotated coordinates, variables with large absolute $\hat{R}$ values, which are considered significant, and variables with near-zero $\hat{R}$ values, which are not significant.

Generally, rotating the PC coefficients only unveils patterns in the $\hat{R}$ matrix. No causal inferences can be made unless measurements (variables) in the original data have similar physical meanings. Because amplitude at different frequencies indicate seismic reflection strength as a function of frequency, the calculated spectral PCs are indicative of the reflection characteristics of the under-resolved thin layer, i.e., the layer thickness.

D: Trace-based Spectral PC and Thin-layer Thickness

The PCA decomposes input data into several independent subsets, i.e. PCs, based on different correlation relationships or "clusters". Assuming that the post-stack seismic data (*s*) is described by the convolution model (Liner, 2004),

$$s = r \otimes w + n \tag{10}$$

where $\otimes$ denotes convolution, the clustering behavior between spectral traces may originate from the reflection series (*r*), the wavelet (*w*), or random noise (*n*). By assuming that noise is random in both the time and frequency domains, and no frequency notch is present in the wavelet, clustering in spectral traces could only be inherited from the reflectivity series.

Spectral amplitude clusters in reflectivity series originate from seismic top-base interference ("tuning") from thin layers and resultant frequency notches. A frequency notch forms when reflections from the top and bottom of a layer interfere destructively. The frequency of a spectral notch is directly determined by the travel time along the layer (Partyka et al., 1999). Similar to the tuning behavior in the time-domain (Widess, 1973; Kallweit and Wood, 1982; Chung and Lawton, 1995), the even- and odd-pair reflections have different tuning frequencies in the frequency domain. For the pure odd- and even-pair reflection pairs (reflection on top and bottom having the same magnitude) of time thickness Δt, the most destructive frequency (F_{des}) occurs at:

(1) for top-base reflections with same magnitude and opposite signs, i.e., a reflection "odd pair":

$$F_{des} = \frac{N}{\Delta t} \quad ; \tag{11a}$$

(2) for top-base reflections with same magnitude and equal signs, i.e., a reflection "even pair":

$$F_{des} = \frac{N + 0.5}{\Delta t} \tag{11b}$$

where $N = 0, 1, 2, 3$ etc. (Marfurt and Kirlin, 2001).

It can be deduced from (11) that there are at least three significant frequency-dependent amplitude clusters in spectral amplitude datasets of an arbitrary thin layer: the non-notch-frequency related amplitude, odd-pair tuning related amplitude, and even-pair tuning related amplitude. They are assumed as the three most significant PCs from TSPCA for each trace.

Practically, in Step (5) of the TSPCA scheme in section *B*, the top three spectral PCs outputted are individually interpreted on the basis of rotated PC coefficients over frequency, and then recorded into three PC images designated for the three clusters. Particularly, the even- and odd-pair tuning related PCs are directly related to the thickness of the under-resolved thin layer, and hence could be used to estimate thickness.
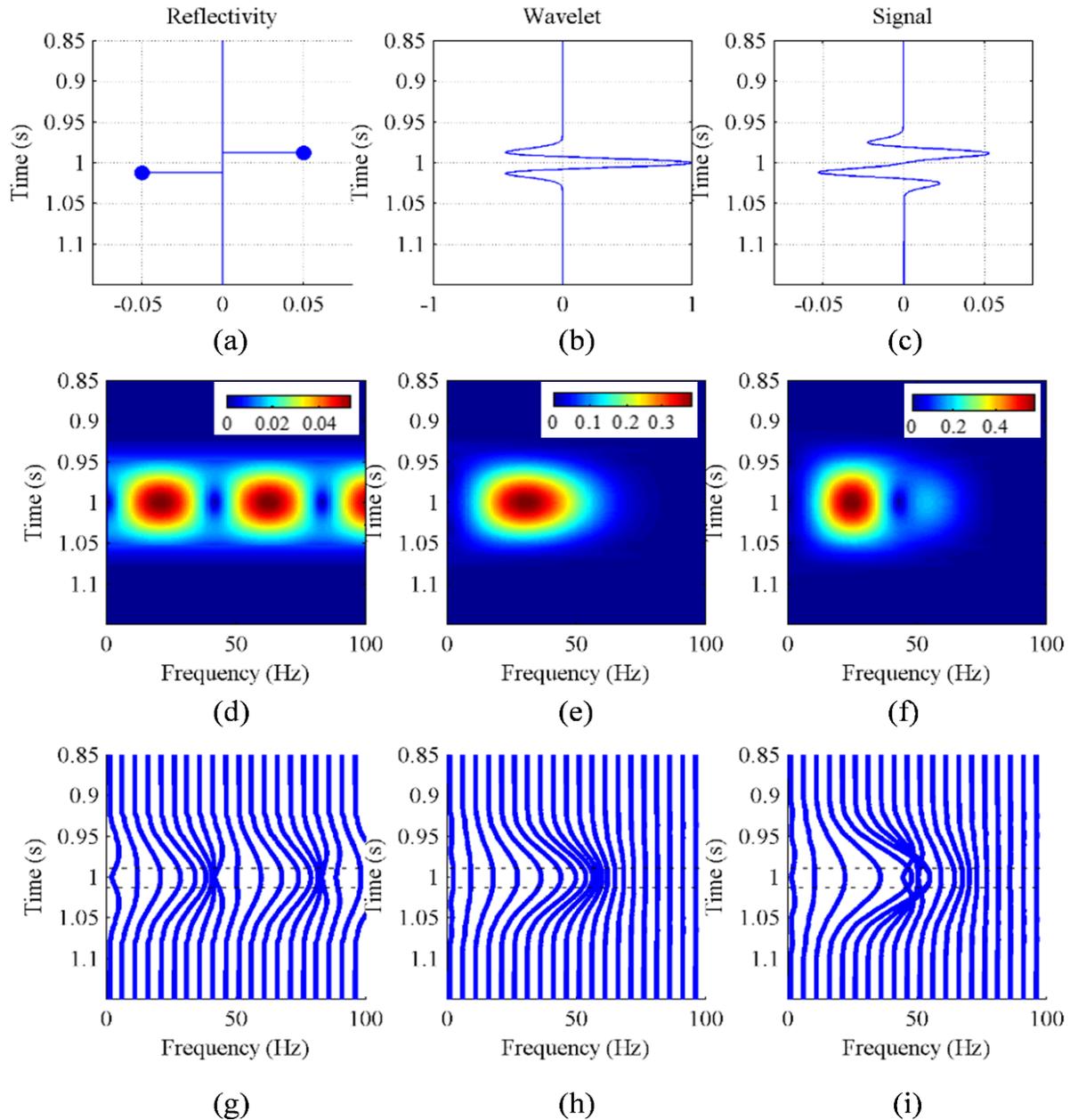

Fig. 4. Spectral decomposition of reflectivity (one 24-ms-thickness layer), 30 Hz wavelet, and signal. Time view of (a) reflectivity, (b) wavelet, and (c) signal. Spectral energy-density view of (d) reflectivity, (e) wavelet, and (f) signal. Iso-frequency trace view of (g) reflectivity, wavelet, and (i) signal.

E. Validation of the TSPCA Method

The TSPCA method is validated using an example that includes one layer of 24 ms time thickness that has the same-magnitude and opposite-sign reflection coefficient on top and bottom. The synthetic seismic signal is created by convolving the reflectivity with a 30 Hz Ricker wavelet [Fig. 4(a)]. Spectral notches are apparent in both reflectivity and signal within the bandwidth of the wavelet as shown in the conventional energy-density [Fig. 4(b)] and spectral-trace [Fig. 4(c)] display. Spectral traces at notch frequencies show poor correlation to those not at notch frequencies. This is represented by lower correlation coefficients at notch frequencies in Fig. 5(b), which is determined by the layer time thickness (e.g., 42 Hz for 24 ms thin layer). Because the wavelet does not have any frequency notch [Fig. 5(a)], the correlation matrix of the signal is almost identical to that of the reflectivity series within the bandwidth of the wavelet.
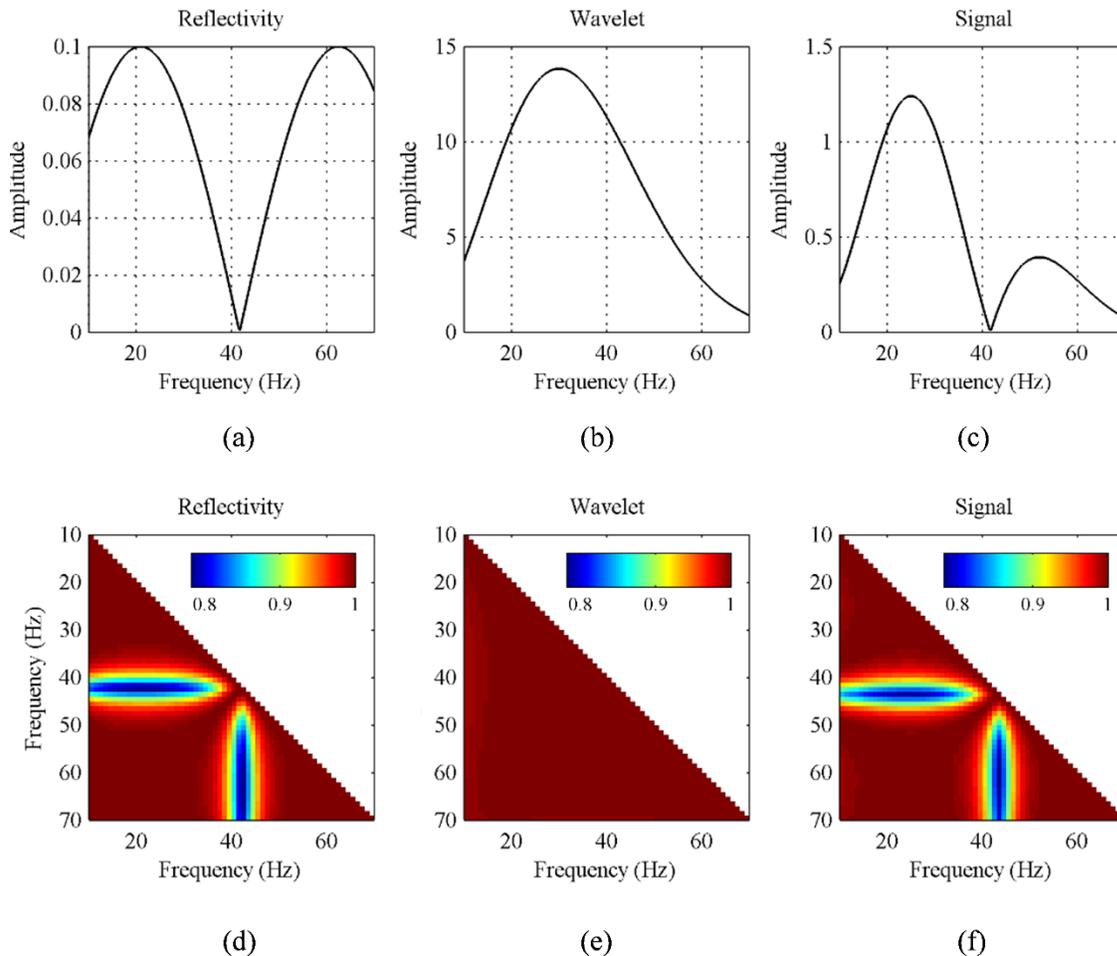
Fig. 5. Spectral notch in amplitude spectrum of (a) reflectivity, (b) wavelet, (c) signal, and spectral correlation matrix of (d) reflectivity, (e) wavelet, and (f) signal.

After eigendecomposition of the input spectral data following (2), the independency of two PCs is shown by comparing the reconstructed correlation matrix using only PC1 or PC2 (R_1 and R_2), following (3). The reconstructed r matrix using PC1 resembles the original correlation matrix (Fig. 6), confirming that PC1 contains most of the information in the original data. However, the PC2-reconstruced correlation matrix displays a different pattern to that of PC1 and the original correlation matrix. Due to its poor correlation to PC1 and low eigenvalue, PC2 could be removed as noise by conventional PC approximations approaches. However, it contains important information that is significant at notch frequencies, i.e., regarding the thickness of the layer. In addition, Fig. 7 shows that the reconstructed correlation matrix using un-rotated and rotated PC coefficients of the first two PCs are similar to the original correlation matrix. This suggest the PCA and Varimax rotation criterion have not added or removed information compared to the original data. Hence, further analysis based on rotated PC coefficients are representative of the original data.
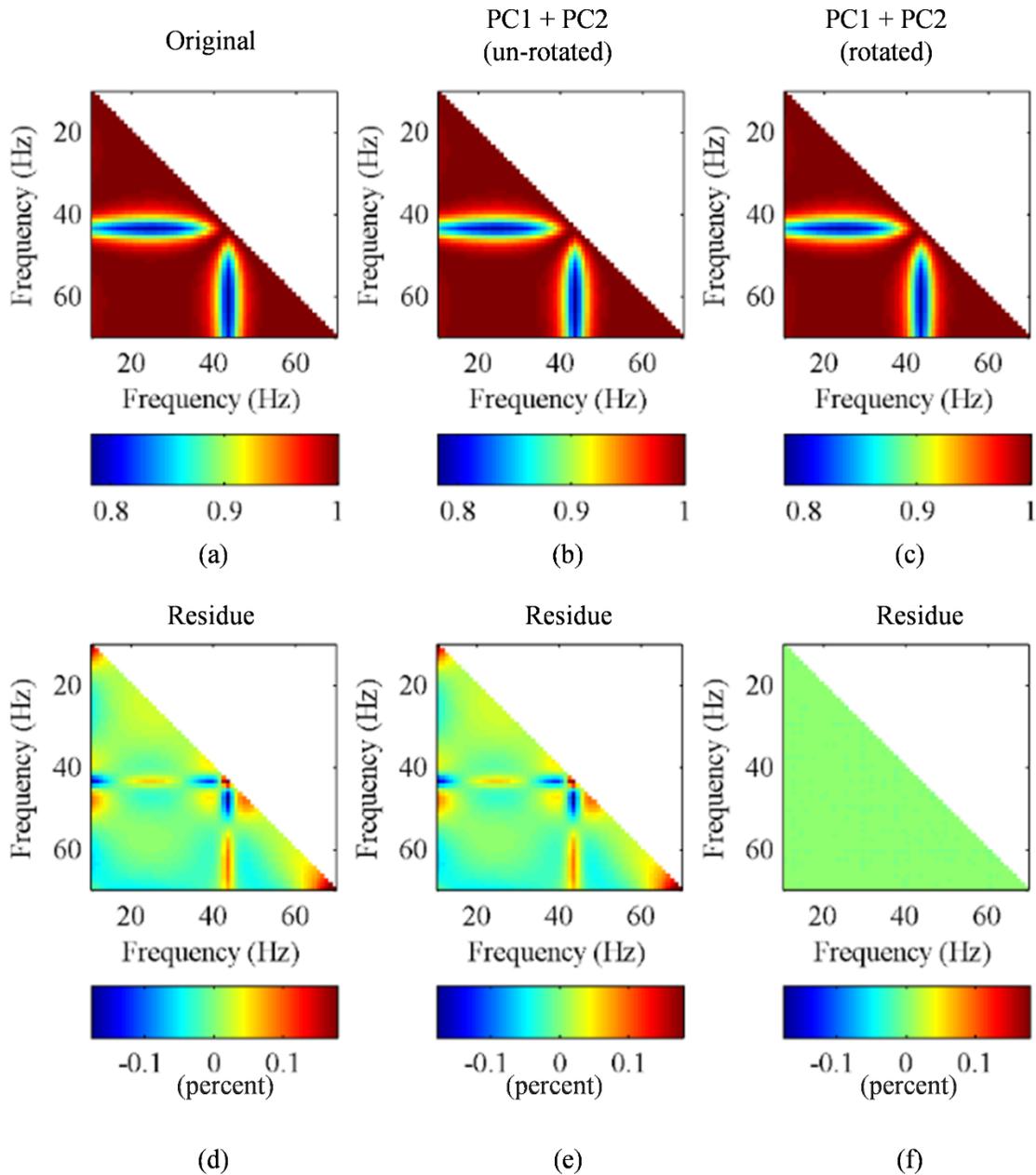

(a) (b) (c)
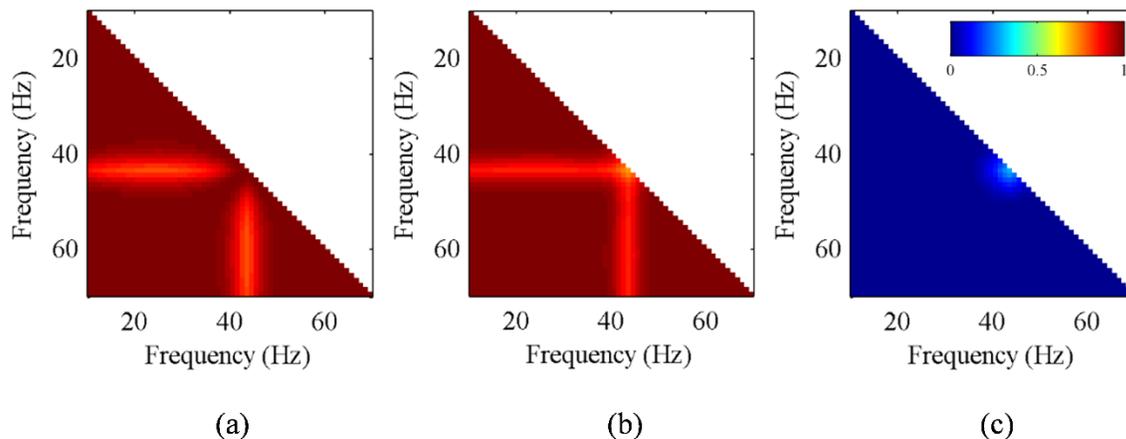
Fig. 6. Original and reconstructed spectral correlation matrix using one PC. (a) Original. (b) Reconstructed with only PC1. (c) Reconstructed with only PC2.

The process of PC coefficient Varimax rotation is demonstrated in Fig. 8. Compared to the original eigenvector and PC coefficients, the rotated PC coefficients show a more distinct variation, making any coefficient-based automated interpretation easier. In this example, PC1 represents amplitude of non-tuning frequencies, while PC2 shows amplitude at tuning frequencies in Varimax rotated PC coefficients [Fig. 8(d)]. In addition, in the general case of a thin layer that contains arbitrary reflection pairs on top and base, which can be considered as summation of a pure even- and odd-pair, PC2 and PC3 are assumed to represent either the even or odd pair reflection amplitude based on their characteristic frequency.

Finally, Fig. 9 compares the (a) original seismic, (b) iso-frequency amplitude traces, and (c) spectral PC traces calculated from (5). The peaks

of both PC1 and PC2 traces are located at the center of the thin layer, suggesting that the output TSPCA traces are truly an attribute of the layer property as opposed to a single reflection event. As shown by Fig. 8(d), the two output spectral PC traces are conceptually similar to the original signal processed using a bandpass filter. However, while the parameters of conventional band-pass filter are arbitrarily, the TSPCA is entirely data driven, and hence has a greater sensibility to thin-layer tuning behavior. Application of TSPCA for thin-layer thickness estimation is tested using the following examples.

Fig. 7. Original and reconstructed spectral correlation matrix using un-rotated and rotated PCs. (a) Original. (b) Reconstructed with PC1 and PC2 in the original coordinates; (c) Reconstructed with PC1 and PC2 in the rotated coordinates after Varimax; (d) Residue of (a) and (b); (e) Residue of (a) and (c), (f) Residue of (b) and (c).
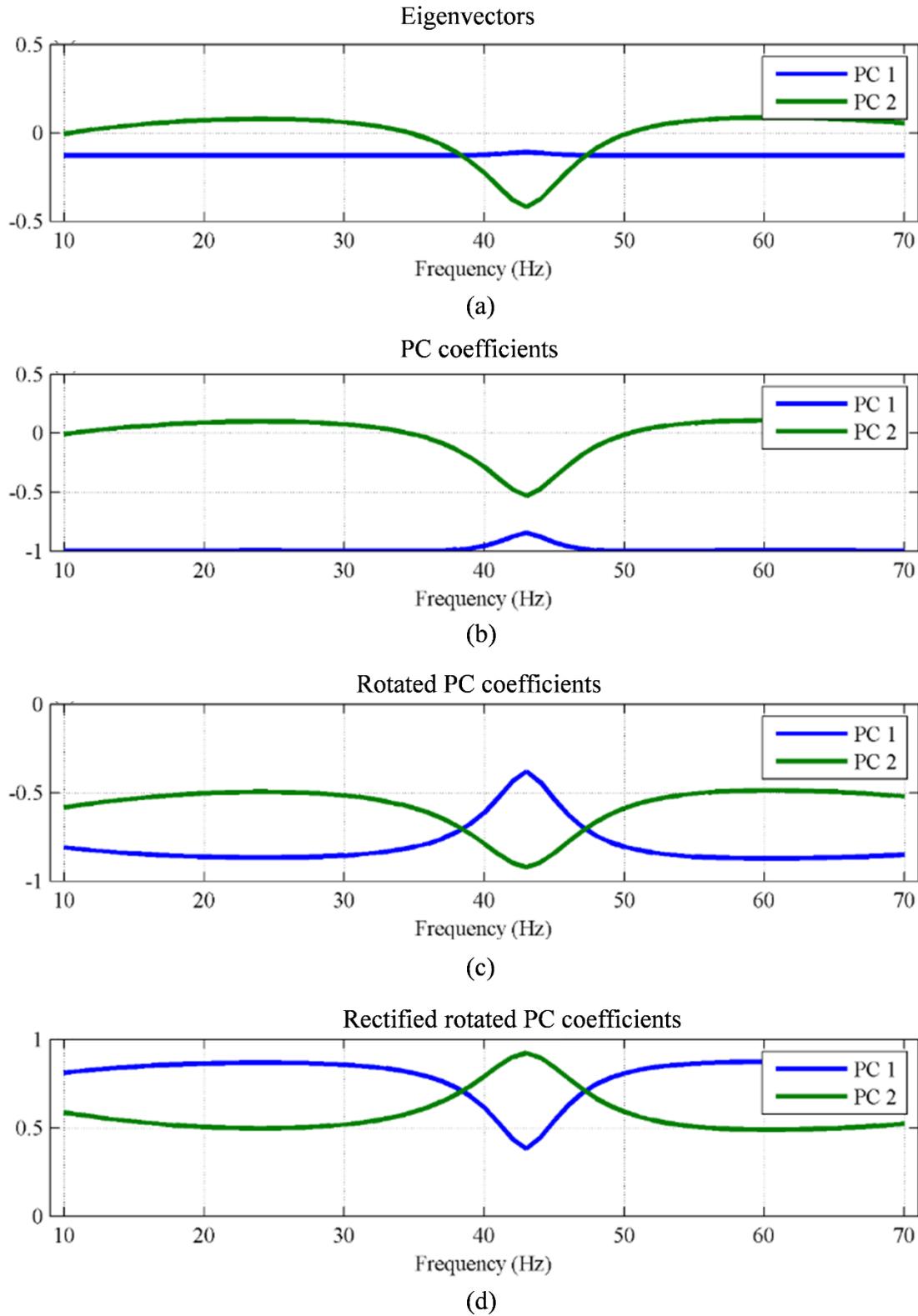
Fig. 8. Varimax rotation of PC Coefficients. (a) Eigenvector. (b) PC coefficients ($\hat{R}$).
(c) Varimax-rotated PC coefficients ($\hat{R}_v$). (d) Rectified rotated PC coefficients ($\left|\hat{R}_v\right|$).
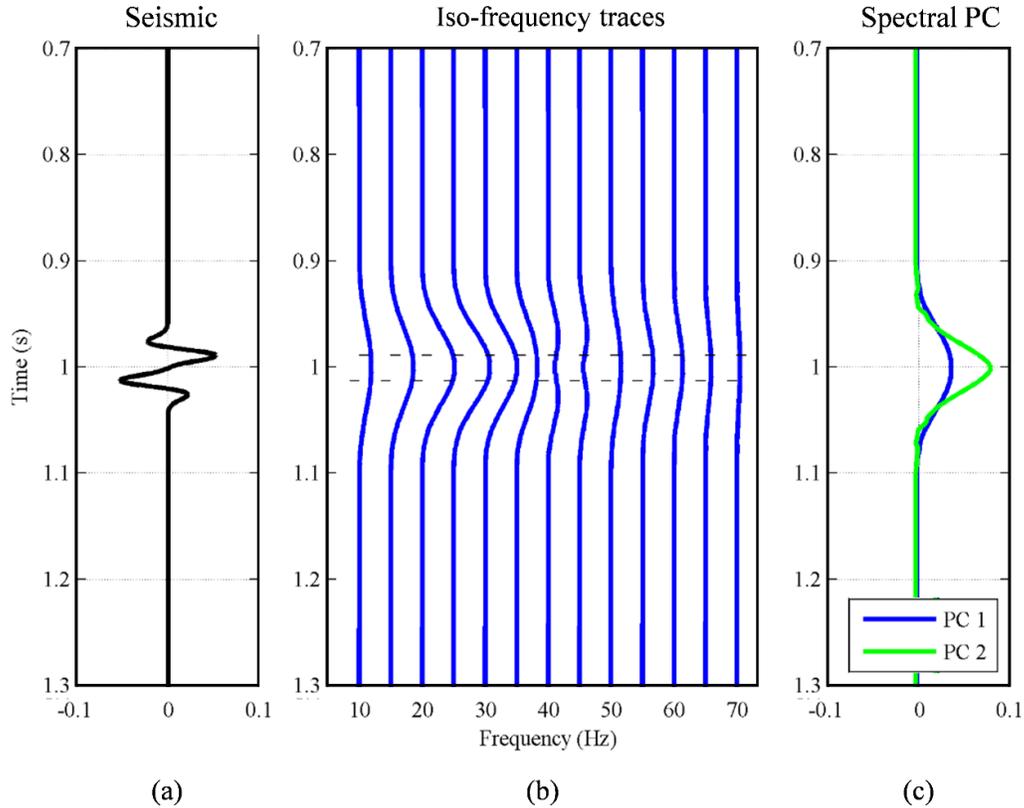
Fig. 9. Trace-based PCA of signal. (a) Seismic signal from the one-layer model.
(b) Iso-frequency traces.   (c) The first and second spectral PC traces.

DATA TEST

A. Wedge Models

To demonstrate trace-based spectral PCA for thickness estimation, two wedge models with pure odd and even reflections are used. Fig. 10 shows the true impedance model and seismic reflection signal when the model is convolved with a 30 Hz Ricker wavelet. As time thickness approaches zero, the reflections from the top and base of the layer interfere and eventually become one new waveform, i.e., the first derivative of the original wavelet. After spectral decomposition and TSPCA, the PC trace and peak amplitudes of PC1 and PC2 are plotted against thickness (Fig. 11).

Firstly, the PC1 trace shows a relative small amplitude variation, whereas the amplitude of the PC2 trace strongly increases as the thickness approaches zero (Fig. 11). This supports a previous assumption, based on Varimax-rotated PC coefficients, that the PC1 and PC2 traces represent the impedance contrast and the wedge thickness variation, respectively. The correlation between the PC2 amplitude and thickness is most apparent when

the layer thickness is less than the tuning thickness of the wavelet, where the top-base interference and waveform distortion occur. The maximum PC amplitude occurs at zero thickness, where the waveform distortion is high. When the thickness is large, the layer top-base interference no longer occurs, and the TSPCA amplitude is insensitive to thickness variation (Fig. 10).
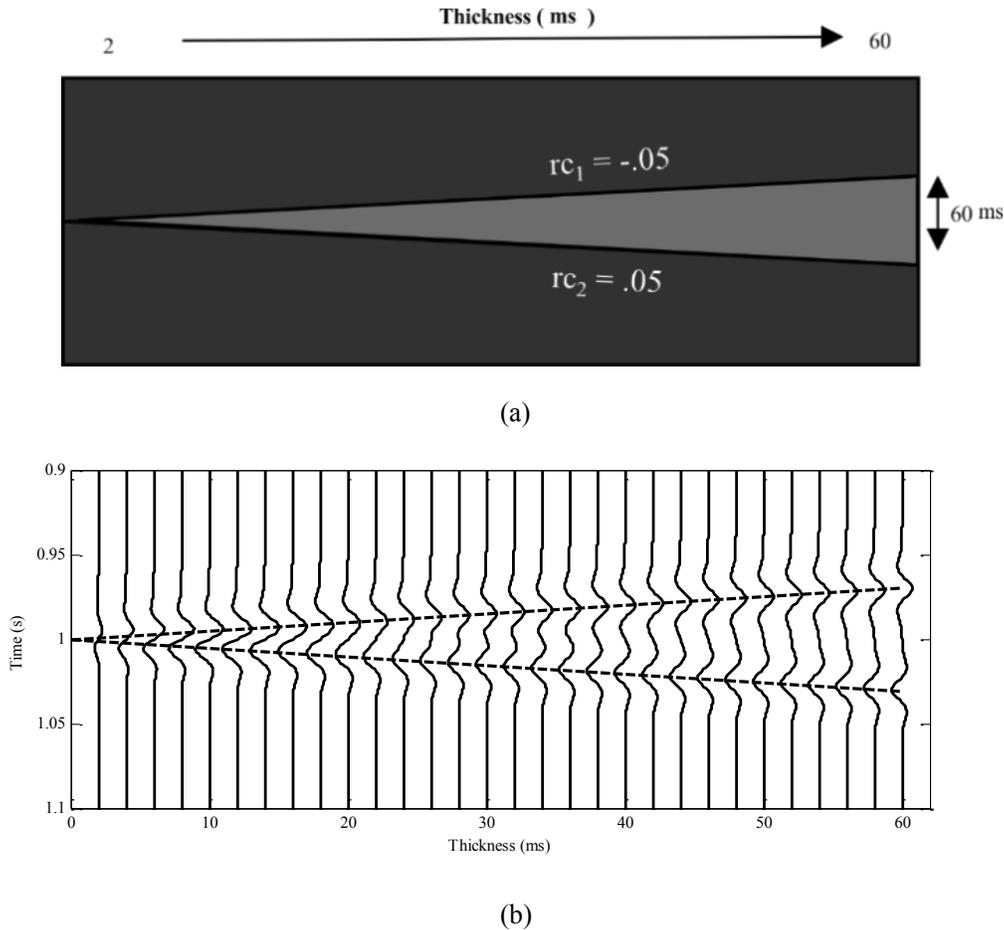

(a)

(b)

Fig. 10. Odd-pair wedge model and signal. (a) Synthetic model containing one wedge with lower impedance. (b) Seismic traces generated from the model using a 30 Hz Ricker wavelet.

In the case of a model with an even reflection pair (Fig. 12), PC1 remains relatively constant as a function of thickness, whereas PC2 shows a high amplitude around the tuning thickness (Fig. 13), differing from the odd case shown in Fig. 11. This might be the result that the waveform distortion appears around the tuning thickness when the top and base reflection have the same polarity, while at zero thickness, the waveform is essentially the same as the original wavelet with twice the amplitude.
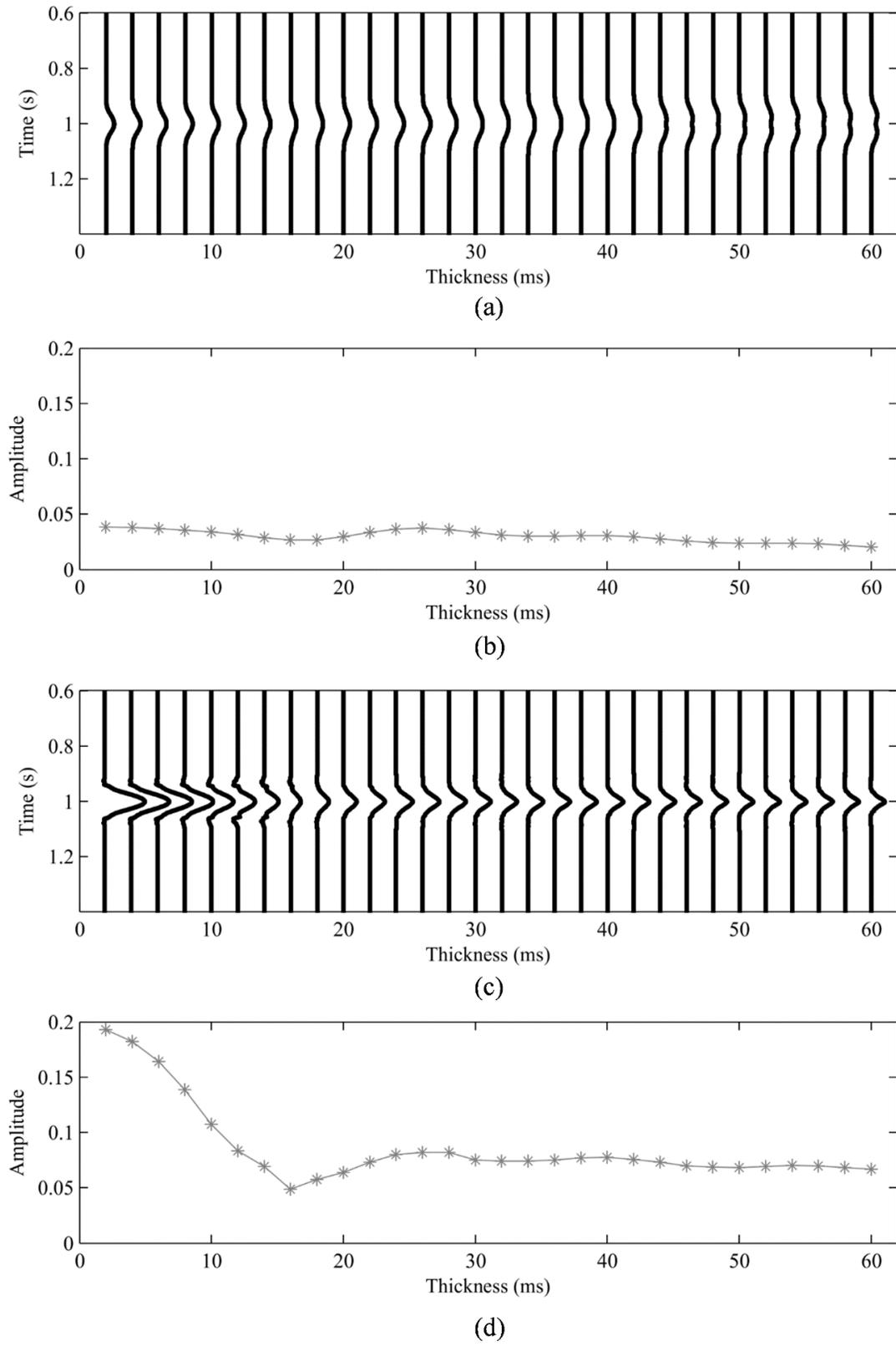
Fig. 11. TSPCA of the odd-pair wedge model signal (a) PC1 traces. (b) PC1 peak amplitude. (c) PC2 trace. (d) PC2 peak amplitude.

Thickness (ms)
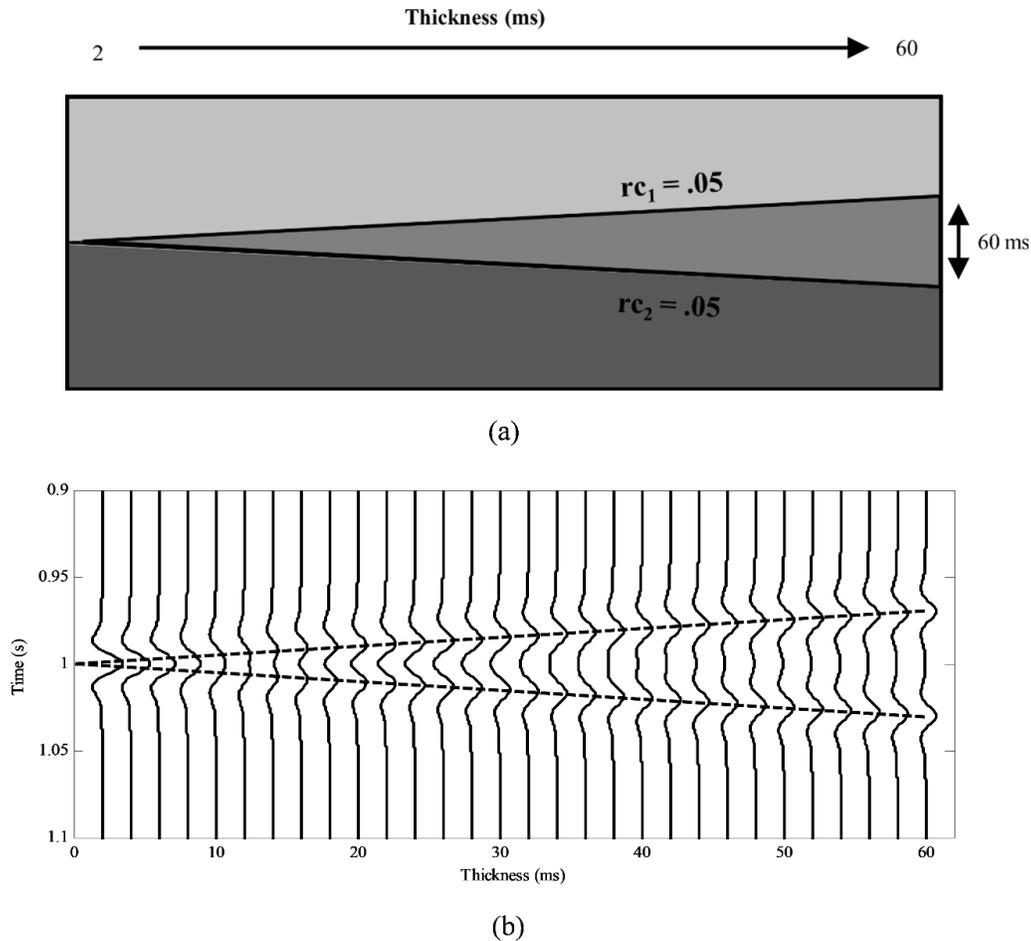
2 ⟶ 60

$rc_1 = .05$

60 ms

$rc_2 = .05$

(a)

(b)

Fig. 12. Even-pair wedge model and signal. (a) Synthetic model containing one wedge with medium impedance. (b) Seismic traces generated from the model using a 30 Hz Ricker wavelet.

B. Complex-geology 3D Channel Model

Fig. 14 shows a more complex 3D synthetic model representing thickness variations of a channel in a non-flat horizon. From the time-structure map, the horizon from which the channel is picked is located on top of a dome-like structure. The second complexity lies in that the channel is deeper compared to the rest of the channel and floodplain area, but does not have a larger thickness. Contrary to the conventional "rule-of-thumb" in seismic amplitude analysis, Fig. 14 shows that the amplitude of the channel at the picked horizon does not necessarily coincides with the true channel thickness from the impedance model. This is due to the low temporal resolution of the original seismic signal. Fig. 15 shows in details the complex structure in the impedance model along two 2D profiles as shown in Fig. 14(a).
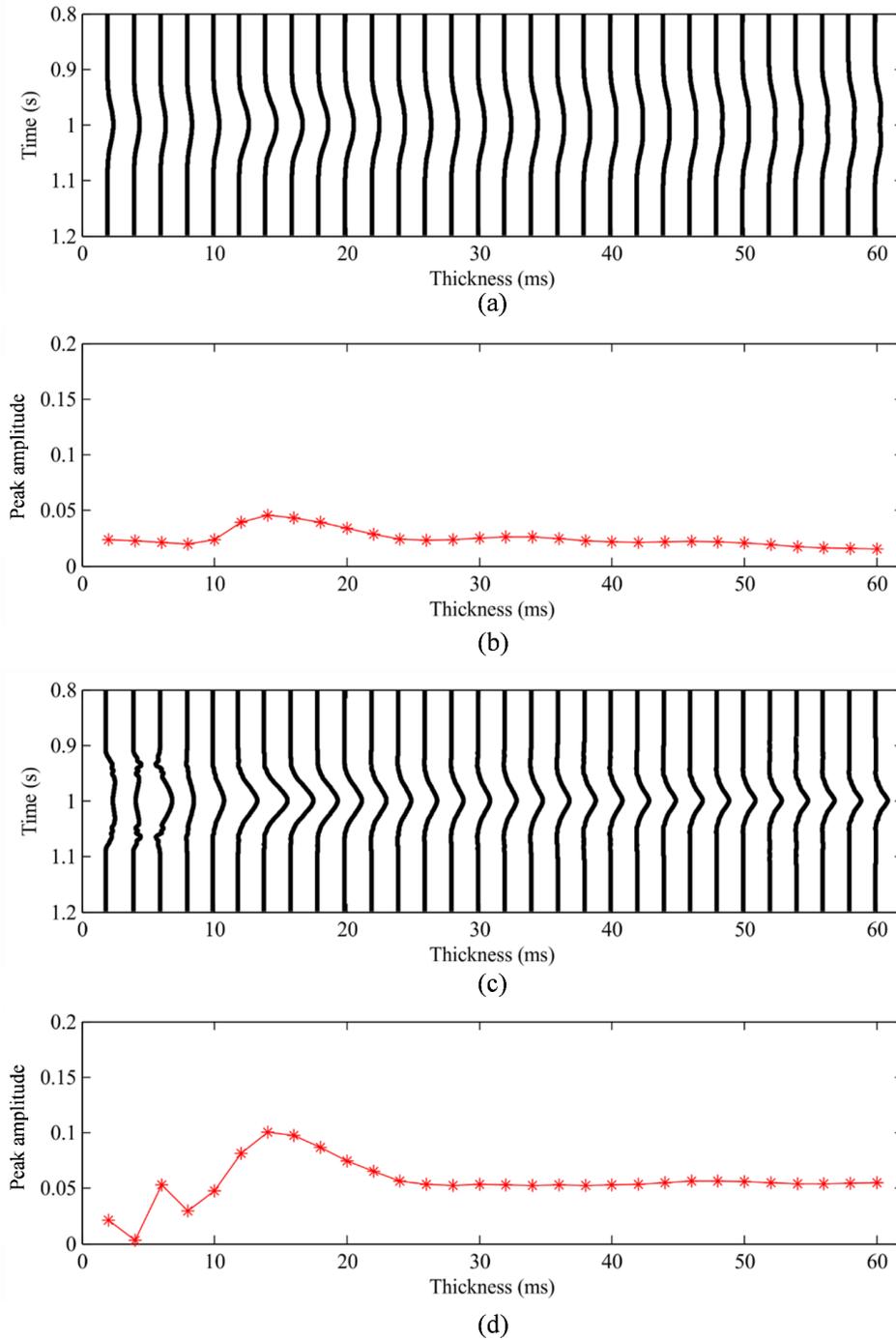
570

Fig. 13. TSPCA of the even-pair wedge model signal (a) PC1 traces. (b) PC1 peak amplitude. (c) PC2 trace. (d) PC2 peak amplitude.

The seismic signal is then spectrally decomposed using a Fourier Transform (STFT) algorithm with a 120 ms time window. Amplitude of the conventional iso-frequency spectral images are affected by the complexity of the model (Fig. 16). Following a conventional HSPCA, the first three PCs

were selected because they have eigenvalues greater than 1, which is often considered a threshold. The calculated horizon-based spectral PC images (see Fig. 17) show that the three PC images present similar overall patterns, especially for PC1 and PC2. The PC3 image highlights the incised valley between xline 140-185. However, compared to the true thickness model and time structure map [Figs. 14(b) and (c)], it is apparent that the highlighted event results from the relative depth of the channel from the incised shape of the valley, instead of the thickness variation.
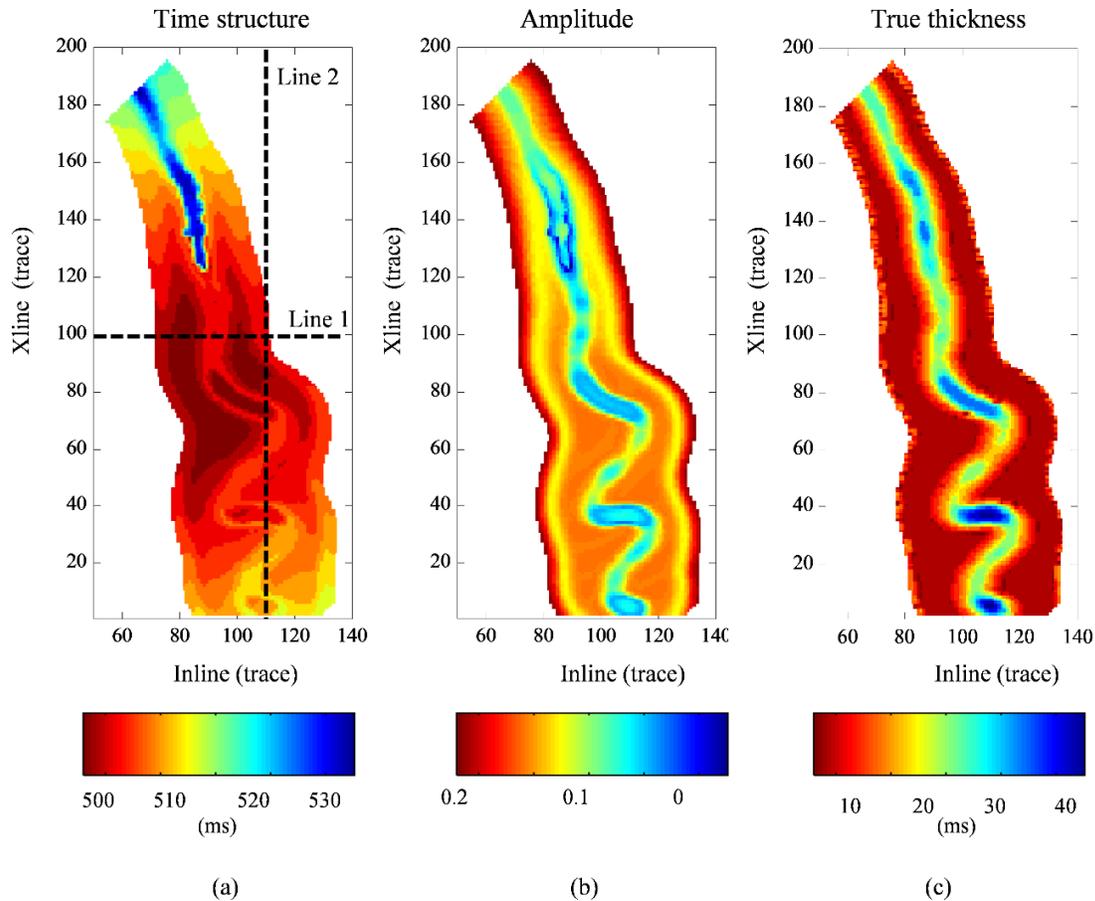
Fig. 14. Complex 3D channel model in map view. (a) Time-structure map of the channel-containing horizon. (b) Signal amplitude at the horizon. (c) True channel thickness.

The result of the TSPCA using a 120 ms time window centered at the same horizon is illustrated in Fig. 18. Amplitude images of the first three spectral PCs show good overall continuity while conforming to the true channel thickness in the model. Spectral PC1 shows little amplitude change, similar as in the wedge models [Fig. 11(b) and Fig. 13(b)]. PC2 and PC3 trends represent amplitudes from the even- and odd-pair models, respectively. High amplitude in the PC2 image between xline 70-80 and 35-40 coincide with parts of the channel with thickness around the tuning

thickness, while the PC3 image exhibits high amplitude at zero thickness. Furthermore, Fig. 19 show true layer thickness associated with the channel cross-plotted with the TSPCA amplitudes. Mean peak amplitude of PC2 and PC3 show good correlation to thickness as observed in the pure even- and odd-pair reflection wedge model, respectively. Error bars show one standard deviation from the mean values. This slight scattering might due to low STFT resolution and slight structure complexity as shown in Fig. 15.
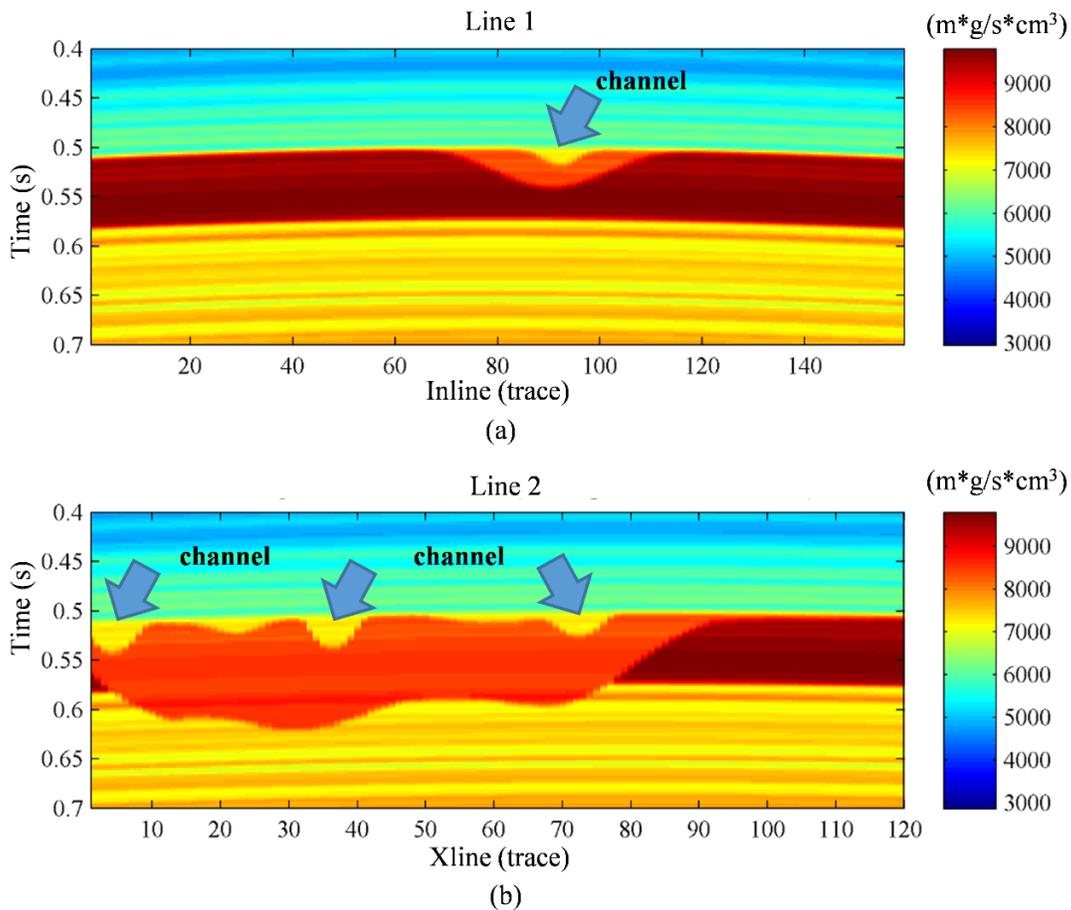
Fig. 15. True model impedance along two 2D profiles in Fig. 14(a). (a) Line 1. (b) Line 2.

One unique property of TSPCA is that it depends on the waveform shape, which indicates the degree of tuning and hence the layer thickness. This differs from the conventional HSPCA. Furthermore, after proper trace scaling and spectral balancing, only the reflectivity spectrum shape is evaluated. The TSPCA result can be independent of the trace amplitude variations which can be affected by wave propagation as well as impedance variations. On the other hand, when there are only subtle changes in waveform shape, a high signal-to-noise ratio of the input signal would be required for the TSPCA to be stable. In addition, high-resolution spectral decomposition would also be preferred to ensure clear PC images.
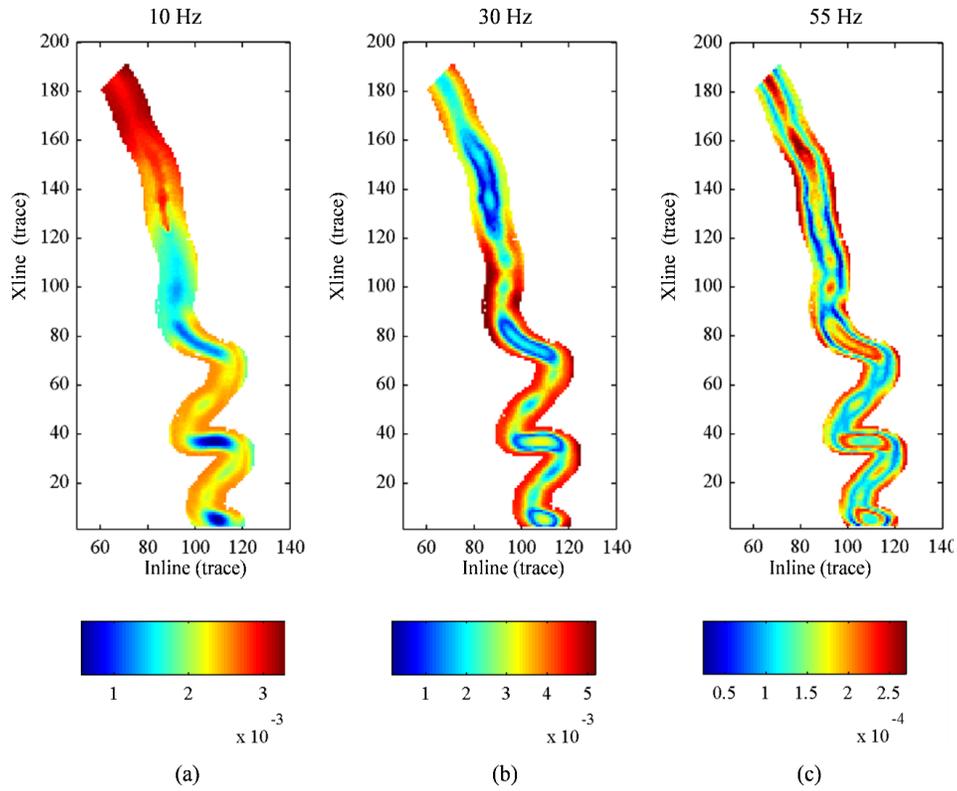
Fig. 16. Iso-frequency images of the channel. (a) 10 Hz. (b) 30 Hz. (c) 55 Hz.
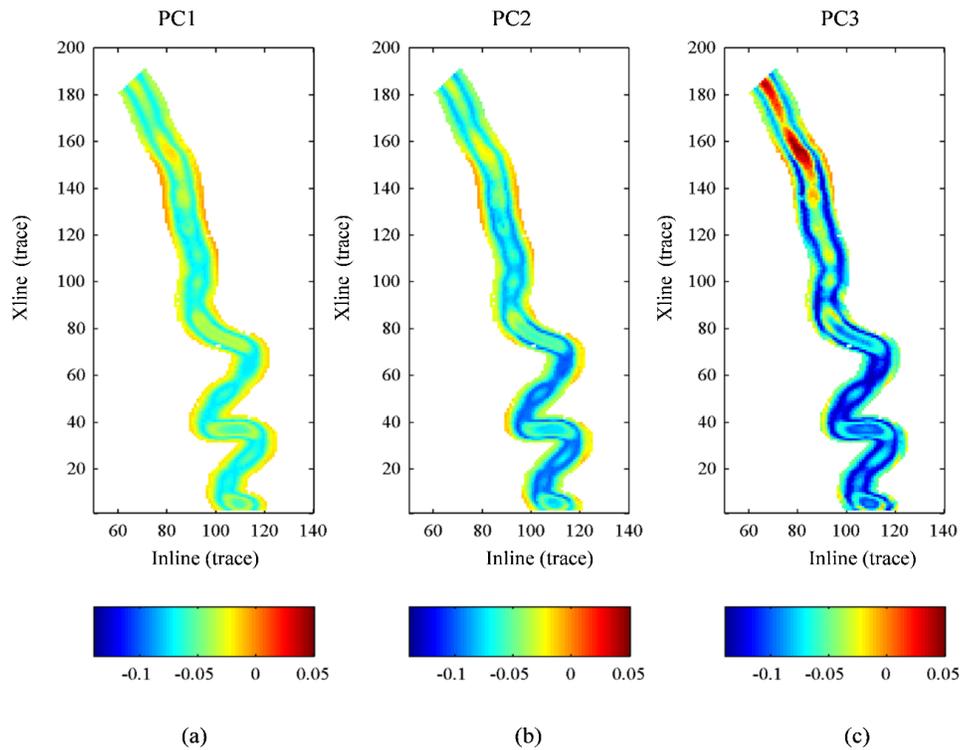

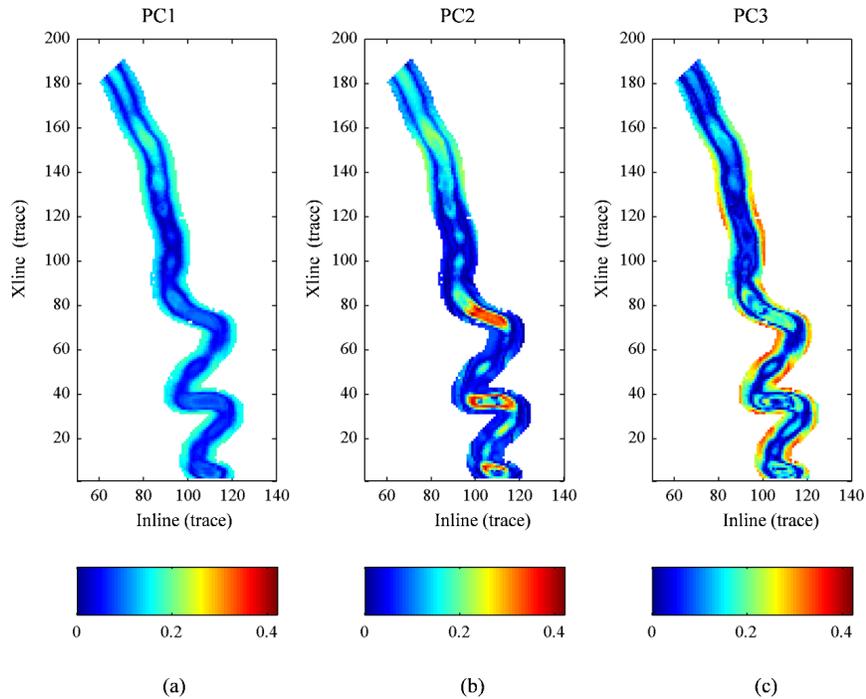Fig. 17. HSPCA images of the channel. (a) PC1. (b) PC2. (c) PC3.

Fig. 18. TSPCA images of the channel.　(a) PC1.　(b) PC2.　(c) PC3.

CONCLUSION

This work proposes a novel trace-based spectral PCA approach for seismic thickness delineation of thin layers using spectrally decomposed seismic signals. Compared to the conventional horizon-based spectral PCA, which overlooks time-variant amplitude information in spectral data, the trace-based approach takes advantage of the correlation between spectral traces that is closely related to the thin-layer thickness. A Varimax rotation of the PC coefficients shows superiority in interpreting significant PCs automatically on a trace-by-trace basis. Results from two synthetic wedge models and a geologically realistic 3D synthetic model suggest that the TSPCA is capable of delineating true thickness variations below tuning more accurately compared to the conventional HSPCA, despite complex geology including subtle thickness change within channel.
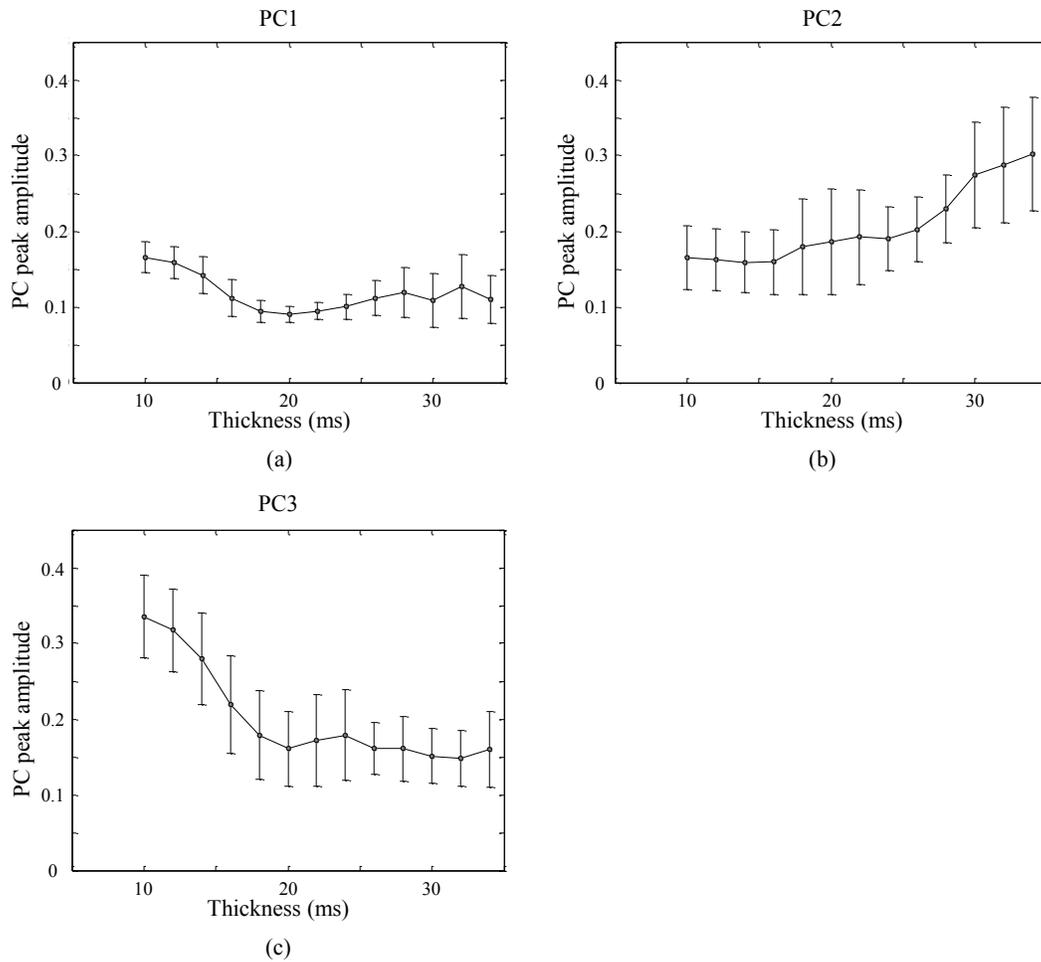
ACKNOWLEDGMENTS

Fig. 19. Trace-based spectral PC amplitude and true model thickness cross-plot. (a) PC1. (b) PC2. (c) PC3.

REFERENCES

Carcione, J.M., Qadrouh, A.N., Perroud, H., Gei, D., Ba, J. and Picotti, S., 2018. Seismic attenuation, normal moveout stretch, and low-frequency shadows underlying bottom simulating reflector events. Geophys. Prosp., 66: 857-871.

Castagna, J.P., Sun, S. and Siegfried, R.W., 2003. Instantaneous spectral analysis: Detection of low-frequency shadows associated with hydrocarbons. The Leading Edge, 22: 120-127.

Chen, G., Matteucci, G., Fahmy, B. and Finn, C., 2008. Spectral-decomposition response to reservoir fluids from a deepwater West Africa reservoir. Geophysics, 73(6): C23-C30.

Chen, Y., Zhou, Y., Chen, W., Zu, S., Huang, W. and Zhang, D., 2017. Empirical low-rank approximation for seismic noise attenuation. IEEE Transact. Geosci. Remote Sens., 55: 4696-4711.

Chung, H. and Lawton, D., 1995. Amplitude responses of thin beds: Sinusoidal approximation versus Ricker approximation. Geophysics, 60: 223-230.

Cohen, L., 1989. Time-frequency distributions-a review. Proc. IEEE, 77: 941-981.

Fomel, S., Landa, E. and Taner, M.T., 2007. Poststack velocity analysis by separation and imaging of seismic diffractions. Geophysics, 72(6): U89-U94.

Gao, J., Dong, X., Wang, W.-B., Li, Y. and Pan, C., 1999. Instantaneous parameters extraction via wavelet transform. IEEE Transact. Geosci. Remote Sens., 37: 867-870.

Gholami, A., 2013. Sparse time-frequency decomposition and some applications. IEEE Transact. Geosci. Remote Sens., 51: 3598-3604.

Guo, H., Marfurt, K.J. and Liu, J.L., 2009. Principal component spectral analysis. Geophysics, 74(4): P35-P43.

Honorio, B.C.Z., Sanchetta, A.C., Leite, E.P. and Vidal, A.C., 2014. Independent component spectral analysis. Interpretation-A. J. Subsurf. Characterizat., 2(1): Sa21-+.

Jolliffe, I., 2002. Principal Component Analysis. Springer Verlag, New York.

Jolliffe, I.T. and Cadima, J., 2016. Principal component analysis: a review and recent developments. Philosoph. Transact. Roy. Soc. A: Mathem., Phys. Engineer. Sci., 374 (2065).

Kaiser, H.F., 1958. The varimax criterion for analytic rotation in factor-analysis. Psychometrika, 23(3): 187-200.

Kallweit, R. and Wood, L., 1982. The limits of resolution of zero-phase wavelets. Geophysics, 47: 1035-1046.

Khare, V. and Martinez, A., 2008. Estimation of sub-tuned reservoir thickness from amplitudes at different seismic bandwidths - a time-domain approach. Expanded Abstr., 78th Ann. Internat. SEG Mtg., Las Vegas: 2968-2972.

Korneev, V.A., Goloshubin, G.M., Daley, T.M. and Silin, D.B., 2004. Seismic low-frequency effects in monitoring fluid-saturated reservoirs. Geophysics, 69: 522-532.

Lawley, D.N. and Maxwell, A.E., 1971. Factor Analysis as a Statistical Method. Butterworths, London.

Levy, S. and Oldenburg, D.W., 1987. Automatic phase correction of common-midpoint stacked data. Geophysics, 52: 51-59.

Liner, C., 2004. Elements of Three-D Seismology. PennWell Books, Tulsa, OK.

Liu, J.L. and Marfurt, K.J., 2007. Instantaneous spectral attributes to detect channels. Geophysics, 72(2): P23-P31.

Marfurt, K.J. and Kirlin, R.L., 2001. Narrow-band spectral analysis and thin-bed tuning. Geophysics, 66: 1274-1283.

Nowak, E.J., Swan, H.W. and Lane, D., 2008. Quantitative thickness estimates from the spectral response of AVO measurements. Geophysics, 73(1): C1-C6.

Partyka, G., Gridley, J. and Lopez, J., 1999. Interpretational applications of spectral decomposition in reservoir characterization. The Leading Edge, 18: 353-360.

Roden, R., Smith, T. and Sacrey, D., 2015. Geologic pattern recognition from seismic attributes: Principal component analysis and self-organizing maps. Interpretation-A, J. Subsurf. Characterizat., 3(4): Sae59-Sae83.

Sinha, S., Routh, P.S., Anno, P.D. and Castagna, J.P., 2005. Spectral decomposition of seismic data with continuous-wavelet transform. Geophysics, 70(6): P19-P25.

Sun, W. and Du, Q., 2018. Graph-regularized fast and robust principal component analysis for hyperspectral band selection. IEEE Transact. Geosci. Remote Sens., 56: 3185-3195.

Wang, Y.H., 2012. Reservoir characterization based on seismic spectral variations. Geophysics, 77(6): M89-M95.

Widess, M.B., 1973. How thin is a thin bed? Geophysics, 38: 1176-1180.

Wiggins, R.A., 1978. Minimum entropy deconvolution. Geoexploration, 16: 21-35.

Williams, G. and Chadwick, A., 2012. Quantitative seismic analysis of a thin layer of CO_2 in the Sleipner injection plume. Geophysics, 77(6): R245-R256.

Zhou, J., Oyem, A. and Castagna, J.P., 2014. An algorithm for frequency-dependent principal component spectral analysis. Expanded Abstr., 84th Ann. Internat. SEG Mtg., Denver: 2636-2640.